

Enhanced sampling of Crystal Nucleation with Graph Representation Learnt Variables

Ziyue Zou¹ and Pratyush Tiwary^{1,2,*}

¹*Department of Chemistry and Biochemistry, University of Maryland, College Park 20742, USA.*

²*Institute for Physical Science and Technology, University of Maryland, College Park 20742, USA.*

(Dated: October 13, 2023)

ABSTRACT

In this study, we present a graph neural network-based learning approach using an autoencoder setup to derive low-dimensional variables from features observed in experimental crystal structures. These variables are then biased in enhanced sampling to observe state-to-state transitions and reliable thermodynamic weights. Our approach uses simple convolution and pooling methods. To verify the effectiveness of our protocol, we examined the nucleation of various allotropes and polymorphs of iron and glycine from their molten states. Our graph latent variables when biased in well-tempered metadynamics consistently show transitions between states and achieve accurate free energy calculations in agreement with experiments, both of which are indicators of dependable sampling. This underscores the strength and promise of our graph neural net variables for improved sampling. The protocol shown here should be applicable for other systems and with other sampling methods.

I INTRODUCTION

The time-scale problem in the computational study of rare events such as protein folding or crystal nucleation with conventional molecular dynamics (MD) simulations is well-known. For many crystal nucleation processes, the simulation time it takes to witness phase transitions can often range from milliseconds to minutes. However, limited by the vibrational motions of hydrogen bonds, the time step of integration of the equation of motion in typical MD simulations is confined to one or two femtoseconds, which means observing one nucleation event requires years of simulation. Obtaining statistically relevant observations on thermodynamics or kinetics becomes out of the question. Many enhanced sampling methods have been proposed to resolve the problems as mentioned above. [1] A larger class of such methods belong to the collective variable family, where relevant slow degrees of freedom for the processes of interest are accelerated in a controllable manner. In popular methods such as metadynamics[2], umbrella sampling[3] or forward flux sampling[4], for practical purposes it is desirable to focus on a maximum of one to three slow degrees of freedom. Ideally these should approximate the reaction coordinate (RC) for the process being studied. [5] In order to design such an approximate RC for the study of rare events, generally one constructs them as a combination of a larger dictionary of features that can collectively distinguish between different metastable states of interest. To mitigate potential ambiguity, we refer to these features as order parameters (OPs) throughout this work.

Over the years a vast range of such hand-crafted and machine-learned OPs have been proposed for the study of crystal nucleation. These can be split into different classes. A first class includes task-specific OPs whose

definitions rely on particular orientations of particles or molecules and their local environments in the corresponding crystalline packings of interest. [6–12] A second class of OPs is more generic and does not need prior knowledge of the relevant crystalline packings. These rely on the computation of the exact or approximated thermodynamic observables. Examples are approximate entropy, enthalpy [13, 14] and moments of coordination number [15, 16]. Given their generic nature, these OPs can be applied to systems without any prior knowledge for the exploration of the free energy landscape and screening of metastable allotropes or polymorphs. However, it is important to note that this generality may occasionally lead to slow convergence and inefficiency in computing free energy. [17]

Different from the above two hand-crafted classes of OPs, recent breakthroughs in machine learning (ML) techniques have given rise to a range of neural network (NN) based OPs for a variety of problems, including crystal nucleation. The inherent differentiability of these OPs makes them suited for various enhanced sampling methods that involve the modification of a system’s Hamiltonian. [18–26] We specifically highlight graph neural networks (GNNs) which have emerged as powerful tool in the realm of materials science, including but not limited to efficient descriptions of material energetics [27, 28], accurate predictions on material properties [29, 30], and robust classifiers of crystal structures and defects [31–35].

Early work involving graph-theoretic ideas, predating the development of GNNs, was already reported for crystal nucleation. Examples include social permutation invariant (SPRINT) coordinates by Pietrucci and Andreoni [36], smooth overlap of atomic positions (SOAP) fingerprints by Bartók *et al.* [37], and other approaches.[38] In the same vein, carefully designed GNN models can construct an optimal representations of complex molecular systems that are invariant to translational, rotational, and permutational symmetries. Translation and rotation invariance of can be achieved by introducing input fea-

* ptiwary@umd.edu

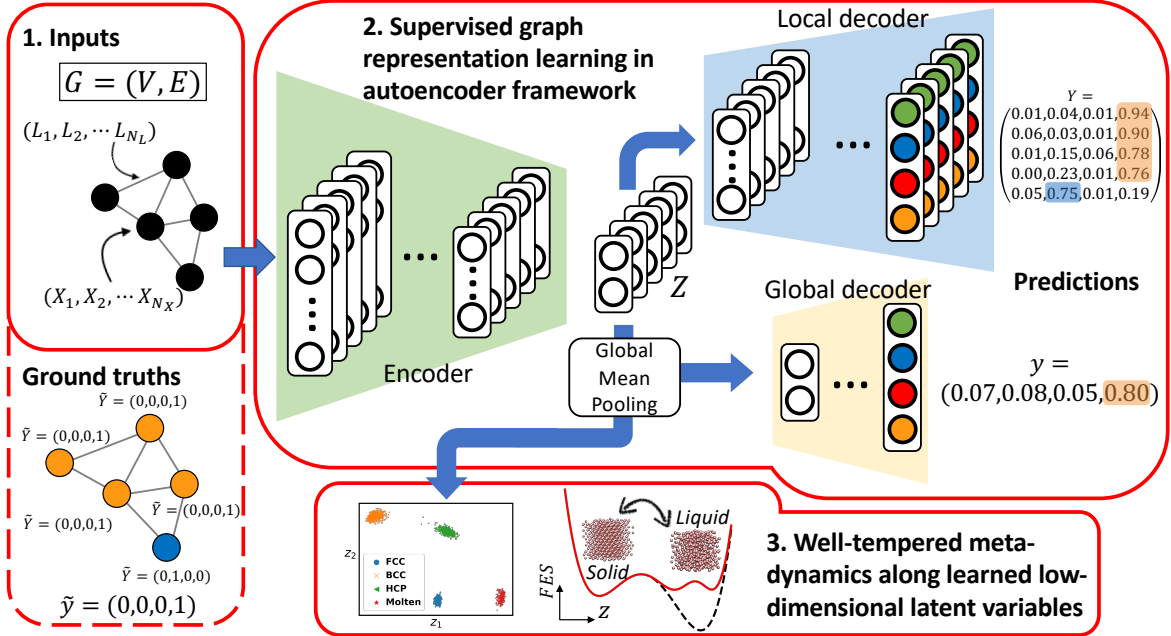


Figure 1. Schematic of the pipeline of the graph representation learning architecture. In part 1, atomic coordinates generated from MD simulations are first converted into graphs consist of tensors of node and edge features (X and L respectively; in solid red box) with labels (in dashed box). In part 2, graph data is fed in the GNN model for the training process. Under a supervised learning scheme, ground truths (i.e. labels) are applied for computing and backpropagating the loss. Once the model is trained, the frozen encoder part along with a global mean pooling layer provides latent variables computed on-the-fly as reaction coordinates for metadynamics (part 3).

tures like radial distances and angles, which themselves remain invariant to both translation and rotation. An example can be found in Ref. 39, which proposed a pre-trained GNN-based representation generator on translation and rotational invariant features with atom-centered symmetry functions for OP construction. On the other hand, in order to classify the overall state of a given structure as a given phase of matter, a natural way is to apply pooling aggregators, where pooling over fully connected layers enforces correspondences between mappings of feature space and classes, and this leads to permutation invariance in GNN models. These properties in combination make GNN models useful in capturing characteristics of the state of highly ordered crystal structures.

While the above approaches are elegant and powerful, there are not yet many approaches where the learned representations from a GNN are biased to enhance the sampling of nucleation processes. The only notable exception is a very recent preprint. [24] In this work, we develop a GNN-based autoencoder framework for acquiring low-dimensional representations that is then used in enhanced sampling of crystal nucleation in two different systems. A GNN model in an encoder-decoder setup is trained to precisely classify crystalline structures using local environments. It ensures permutation, translation, and rotation invariance in its latent outputs. A global

pooling layer achieves invariance to permutational symmetry, while translation and rotation invariances arise from carefully chosen input features. These compact learnt variables can be easily integrated into various enhanced sampling techniques, thanks to the differentiability of machine learning models. To demonstrate the efficacy of our approach, we apply it to two challenging systems, namely iron and glycine, in the context of nucleation from the melt using metadynamics. Our results show the obtained latent variables capture key configurational features from the training dataset and are able to enhance the samplings as evidenced by frequent back-and-forth transitions. Our work has complementary aspects to Ref.24. While we benchmark directly on input atomic configurations, allowing the GNN model to probe their structural differences, the model from Ref.24 provides an accurate and efficient method for reconstructing conventional order parameters by including their information in the loss function. We then conduct comprehensive thermodynamic analyses, focusing on the computation of free energies, which exhibit excellent agreements with existing literature regarding the stability rankings of various allotropic and polymorphic structures.

II METHODS

As introduced above, simulating rare events like crystal nucleation in simulations require both associated progress coordinates and enhanced sampling methods to increase movement along these progress coordinates. Here we provide detailed information on both of these aspects in the following three subsections: we first introduce graphs and graph neural nets in Sec. II A, and we present details on how these graphs are prepared (Sec. II B). Then, we summarize the sampling method well-tempered metadynamics, in Sec. II C. We provide details on setting up the simulations in the SI and descriptions of the notations in the machine learning model in Tab.I.

II.A Graph Neural Networks (GNN) based model

A graph $G = (V, E)$ has two primary components: vertices (or nodes) V and edges E . Node (X) and edge (L) embeddings correspond to labels on vertices and edges respectively. In this work, we use a k-nearest neighbor (kNN) algorithm [40] to construct the neighborhood \mathcal{N}_v where k is a tunable parameter. In Fig. 1 panel 1, a graph with 5 vertices is presented as an example with N_X number of node features and N_L number of edge embeddings, these feature tensors eventually serve as input to GNN models. For simplicity, node features are set to 1 for systems studied in this work and edge features are selected to be translation and rotation invariant (which we discuss in the next subsection, Sec.II B). Models designed in this work adopt a supervised learning scheme which therefore requires ground-truth labels of different crystal phases for computing and minimizing the loss function. The atom-wise labels are generated with different baseline classifying methods and the graph-level label is determined by the leading population of fingerprints on nodes.

As shown in Fig. 1, the learning scheme is composed of three parts: creating graph data, training GNN models to learn low-dimensional order parameters (OPs), and performing enhanced sampling along a further reduced space. In this work this is done through an embedded autoencoder framework that allows one to obtain a low-dimensional representation for generic enhanced sampling methods. Specifically, starting from selected node and edge features (described separately in the next subsection) as input features, the encoder, colored in green in Fig. 1, takes the input and compresses them into a relatively lower-dimensional local descriptor Z . For the applications shown in this work, Z is $(N, 2)$ dimensional, where N is the total number of nodes in a graph. The local descriptor (in blue in Fig. 1) predicts the structure of individual nodes, which could be atoms or molecules, given the information about their neighborhood. In addition, a global decoder, shown in yellow, classifies the entire input graph by coupling it with a global pooling

layer. Here we choose to use the global mean pooling layer which avoids the effect of system size, compared to other schemes such as sum or max poolings. In other words, this makes the trained model size-agnostic (i.e., transferable to systems of the same species of any size). The output of the global mean pooling operation, z , is generally two-dimensional and is biased in enhanced sampling.

The graph convolutional layers, specifically edge-conditioned convolution (ECC) layers [27, 32, 41], allow message passing of node and edge features of the linked neighboring nodes \mathcal{N}_v into the individual vertex through convolution operations, as described in Eq.1:

$$X^l(i) = \frac{1}{|\mathcal{N}_v|} \sum_{j \in \mathcal{N}_v} F^l(L(j, i); w^l) X^{l-1}(j) + b^l, \quad (1)$$

where l is the layer index in the neural network, w and b are learnable weights and biases of the network. A filter network [42] F^l parameterized by weights w outputs an edge-specific weight matrix given edge attributes $L(j, i)$. We keep the same machine learning architecture for the different systems studied in this work. In particular, we keep zero hidden layers in both decoders to maximally optimize the ability of the encoder to classify different crystal structures.

The learning objective \mathcal{L} of this model consists of a sum of two cross-entropy losses provided in Eq. 2, where classes in this work correspond to crystal structures. The first term, which is a local prediction term, computes the cross-entropy loss of the node logits $Y_{i,c}$ of node i class c with respect to the node-level ground truth $\tilde{Y}_{i,c}$ which is intrinsically a binary indicator (0 if the node does not belong to class c and 1 it does so) and then sums over all classes and nodes. The second term, which is a global prediction term, calculates the cross entropy between the c^{th} class graph prediction (y_c) and the target (\tilde{y}_c). A hyperparameter β is introduced to control the relative importance in local and global prediction.

Table I. Notations for the machine learning model used in this paper

Notations	Descriptions
V, X	Nodes and node embeddings
E, L	Edges and edge embeddings
N	Number of vertices (nodes)
\mathcal{N}_v	Neighborhood set of node v
l	Model layer index
F	Edge convolution network in ECC layers
y, Y	Global and local predictions
\tilde{y}, \tilde{Y}	Graph and node labels (one-hot)
Z	Node latent variables
z	Global (pooled) latent variables
\mathcal{L}	Loss function
β	Hyperparameter in loss function

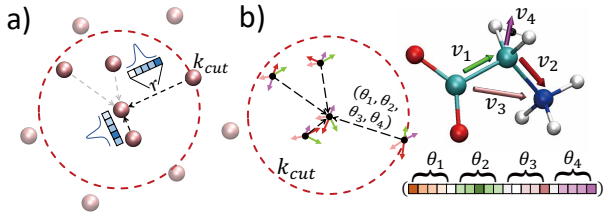


Figure 2. Geometric representations of (a) iron particles and (b) glycine molecules. Gaussian basis functions are applied to featurize edge attributes individually and node features are set to be one for both systems. The neighborhood is defined with the k -nearest neighboring algorithm ($k_{cut} = 4$ as an example). v_i 's are intramolecular characteristic vectors and θ_i 's are the corresponding intermolecular angles formed by specific v_i . v_1 is the C-C $_{\alpha}$ vector, v_2 is the N-C $_{\alpha}$ vector, v_3 is the C-N vector and v_4 is the C $_{\alpha}$ -H $_{center}$ vector. Atoms are colored with respect to their species: irons in mauve, oxygens in red, carbons in cyan, nitrogens in blue, and hydrogens in white. Ghost particles (i.e., center of mass of glycine and center of hydrogen atoms) are in black.

$$\mathcal{L} = - \sum_i^N \sum_{c \in \text{classes}} \tilde{Y}_{i,c} \log Y_{i,c} - \beta \sum_{c \in \text{classes}} \tilde{y}_c \log y_c. \quad (2)$$

II.B Dataset Preparation

Like all data-driven methods, prior information needs to be provided to train our model. In this work, the model uses all-atom coordinates from MD simulations initiated from different perfect crystal structures. The training data for iron allotropes was generated by LAMMPS built-in lattice functional; while the molten phase was prepared by random insertion of iron particles. Separately, four supercells composed of 432 α -Fe, 256 γ -Fe, 180 ϵ -Fe, and 285 molten Fe were constructed and 1 ns short MD trajectories were initiated accordingly. These structures were equilibrated at respective temperatures where they are expected to be stable. Specifically, this was 1000 K for α -Fe, 900 K for γ -Fe, 900 K for ϵ -Fe, and 2000 K for molten Fe. A total of 2000 frames of MD snapshots, corresponding to 500 frames for each configuration, were then converted into graph representation and trained via the proposed model discussed above. The node feature was set to be unity. A sparse adjacency matrix was constructed on k -nearest neighbors (k -NN) metric. [43] Each pair of linked nodes was attributed the radial distance as the edge feature, followed by a Gaussian basis function introduced in Schnet shown in Fig.2a). [28] An edge feature, L , can be obtained by expanding distance, r , into t slices as follows:

$$L_t(\mathbf{x}_i - \mathbf{x}_j) = \exp(-\gamma(r_{ij} - \mu_t)^2), \quad (3)$$

where \mathbf{x}_i is the position tensor for node i , and $r_{ij} = \|\mathbf{x}_i - \mathbf{x}_j\|$ guarantees translation and rotation invariance

of the GNN model.

Crystal structures of glycine polymorphs were obtained from the Crystallography Open Database. [44] In a similar manner as for iron, different supercells consisting of 128 molecules as α -glycine[45], 128 as β -glycine[46], 108 as γ -glycine[45], and 137 as liquid glycine (denoted as ℓ -glycine) were built using unit cells of glycine polymorphs prepared with the Mercury package. [47] MD simulations of all glycine polymorphs were carried out at 300 K ; while the liquid glycine was obtained at around its melting temperature of 500 K . All MD simulations are of length 2 ns and 2000 frames were obtained from each simulation for training the model. Individual glycine molecule is treated as one entity with the corresponding center of mass (i.e., one node per molecule; black dots in Fig.2b)) whose feature is 1. The leading 6 nearest neighbors are defined as neighboring molecules referring to the position of the center of mass of each molecule. Different from iron, edge attributes are concatenations of four intermolecular angles under Gaussian basis function into one long feature vector as shown in Fig.2b) bottom right. The angles are defined by the intramolecular vectors: ν_1 is the C-C $_{\alpha}$ vector, ν_2 is the N-C $_{\alpha}$ vector, ν_3 is the C-N vector and ν_4 is the vector of C $_{\alpha}$ and the geometric center of the two associated hydrogens (see Fig.2b) for illustrations).

II.C Well-Tempered Metadynamics

The low-dimensional latent variables learnt through the global mean pooling operation (Fig. 1) serve as low-dimensional descriptors of various competing phases. Due to the loss function in Eq. 2 these capture both local and global information, making them well-suited for driving short-range and long-range fluctuations relevant to nucleation. Here we do so by performing well-tempered metadynamics (WTmetaD)[48] along these variables, while expecting that our protocol should be fully amenable to other enhanced sampling approaches.

In WTmetaD, history-dependent Gaussians are deposited along pre-defined biasing variables reaction coordinates to facilitate state-to-state back-and-forth transitions between different metastable states the system would normally be trapped in. We refer to Ref.48 for further details of WTmetaD. Here we used the latent variables (z_1, z_2) from Fig. 1 as the variables being biased. Other parameters used in performing WTmetaD simulations are reported in Tab. II. Iron nucleation simulations were performed with LAMMPS-23Jun2022 simulator [49] and glycine simulations were performed with GROMACS-2021.6 MD engine.[50] Both packages were patched to PLUMED-2.8.1 with the Pytorch module enabled. [51, 52] Codes for reproducing the simulations in this work are available at Github.

III RESULTS AND DISCUSSIONS

We evaluate the ability of the GNN-learned low-dimensional latent representations to enhance sampling by performing well-tempered metadynamics for the two selected representative systems, namely, iron (Sec.III A) and glycine (Sec.III B) initiated from their molten or liquid phases. Iron as one of the most abundant elements on Earth has received significant interest given its importance in steels and alloys and in geology. Many allotropes of pure iron exist, which are the body centered cubic (BCC) α -Fe, the face centered cubic (FCC) γ -Fe, the hexagonal close packing (HCP) ϵ -Fe and the BCC δ -Fe. In addition to iron, we assess the reliability of our protocol on the nucleation of polymorphs of the simplest amino acid glycine. This is an important system as physical properties in different glycine polymorphs vary which can change the effect of glycine as an inhibitory neurotransmitter. [53] Furthermore, the existence of many possible space groups complicates the problem in molecular crystals in general.[54] Three polymorphs, namely α -, β -, and γ -glycine, exist in zwitterionic glycines at ambient conditions. In particular, α -glycine (space group: $P2_1/n$) and β -glycine ($P2_1$) are monoclinic and γ -glycine ($P3_1$) is trigonal. We compute free energy differences between these different metastable allotropes/polymorphs and compare with respective literature.

III.A Phase Transitions in Pure Iron

Experimental measures suggest α -Fe remains stable at temperature less than 1184 K ; while γ -Fe is stable between 1184 K to 1665 K . When above 1665 K , γ -Fe transforms to another BCC structure, δ -Fe until sublimation. In addition, the HCP ϵ -Fe is stable at a pressure greater than 13 GPa . [57, 58] The enrichment of crystal packings makes iron a challenging system and an excellent test case for our proposed protocol.

The graph data for iron particles is shown in Fig.2a). Since the system of interest here is in single species, the feature of individual nodes is set to be 1. We set a k-NN cutoff ($k = 50$) that is much larger than the coordination number (number of neighboring particles in the first shell) of close packing structures. This helps gain information from nodes several hops away in order to account for the structural similarities in FCC (abcabc...) and HCP (ababab...) crystals. The edge features are the Gaussian expanded radial distance as introduced in Methods (Sec. II B). The edge feature is an expanded

Table II. WTmetaD Parameters

System	$\omega(k_bT)$	γ	σ_1 (RC unit)	σ_2 (RC unit)	T (K)	pace
Iron	1.0	50	0.2	0.2	1800	500
Glycine	2.0	100	0.15	0.1	500	500

Table III. Free energy differences between melt/liquid and crystal structures sampled in WTmetaD simulation with respect to the initial molten (M)/liquid (ℓ) phases.

System	Transition	Free energy difference (kJ/mol)
Iron	M \rightarrow FCC	52.63 ± 5.63
	M \rightarrow HCP	-20.15 ± 8.52
	M \rightarrow BCC	-34.06 ± 4.20
Glycine	$\ell \rightarrow \alpha$	56.43 ± 16.92
	$\ell \rightarrow \beta$	658.87 ± 74.72
	$\ell \rightarrow \gamma$	234.11 ± 35.41

radius distance in 10 dimensions.

We find that well-tempered metadynamics biasing along the 2-dimensional latent variable learnt from GNN leads to robust, multiple state-to-state transitions without any hysteresis, as can be seen from the time series in Fig.3a). The associated free energy surface is then constructed following the appropriate reweighting scheme. [59] Three distinct energy basins correspond to the initial molten state, HCP iron, and BCC iron (Fig.3b)). On the contrary, no distinct basin is sampled for the FCC state of iron, which suggests such a configuration is thermodynamically less stable at the simulation temperature of 1800 K . This is expected because FCC is reported to be the least stable allotrope among other forms from both experiments [60] and zero temperature calculations [61, 62].

An advantage of the proposed ML model is that its local decoder (Fig.1) provides an estimation, in a probabilistic sense, of the class or crystalline structure of individual nodes belonging to. [6, 64, 65] The populations of different crystal packings can then be computed by the summation of individual weights from the output Y of the local decoder, $N_{class} = \sum_i^N Y_{i,class}$ as shown schematically in Fig.3c). Additionally, we present results in the form of a 2-dimensional free energy surface in the SI for indicators of potential solid-solid transitions. The free energy difference ΔG can be computed between phases and, as an example, the equation between liquid, ℓ , and solid, s , is shown as follows:

$$\Delta G_{\ell \rightarrow s} = -k_B T \ln \left(\frac{\langle H(N_s - N_c) \rangle}{\langle H(N_\ell - N_c) \rangle} \right), \quad (4)$$

where $\langle \cdot \rangle$ is the reweighted unbiased average and H is the Heaviside step function with a size cutoff N_c . The tabulated free energy differences between metastable crystalline states and the starting molten state are plotted in Fig.3d) and reported in Tab.III with a threshold value of 150 in Eq.4, which means frames are categorized into the corresponding state for free energy computation when $N > 150$ (within a total of 285 Fe irons in the box). In addition, Fig.3d) suggests that the WTmetaD simulations performed are well-converged. The values were averaged over four independent production runs of 200

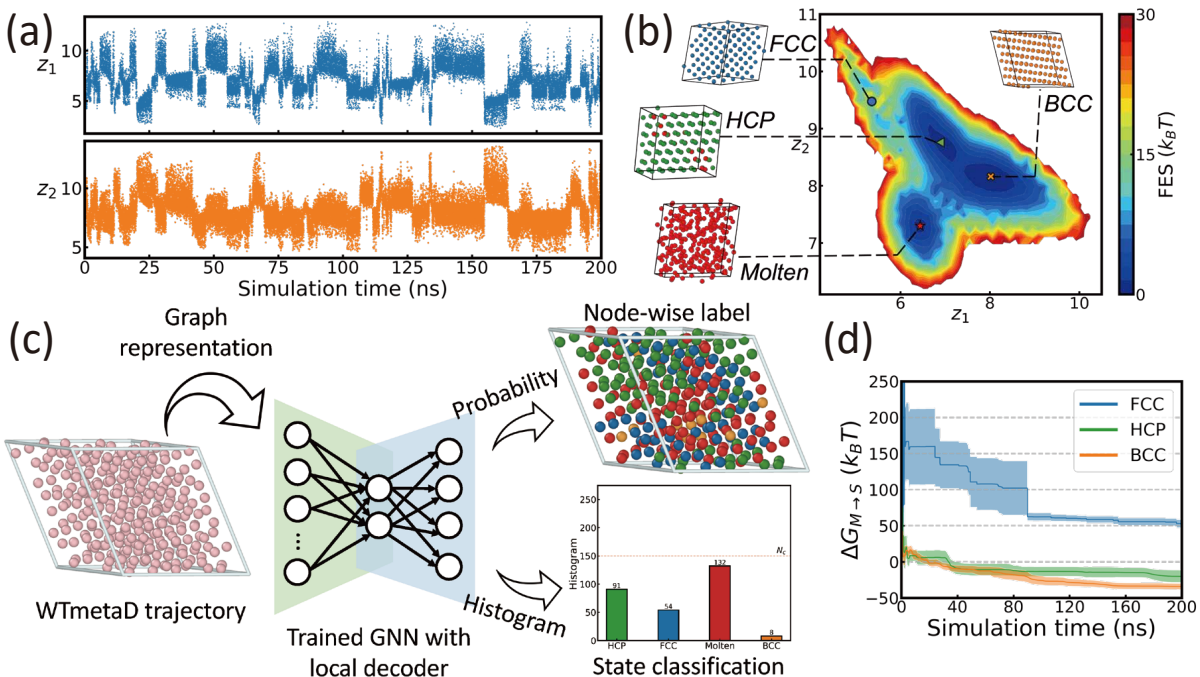


Figure 3. Results of WTmetaD simulations of iron nucleation from its melt. Machine learnt latent representations z_1, z_2 as a function of simulation time in panel a) shows frequent state-to-state transitions. Subplot b) shows reweighted FES (free energy surface) in the latent variable space (z_1, z_2) with landmarks of sampled configurational snapshots from OVITO package. [55] Iron particles are color-coded with respect to the adaptive common neighbor analysis method. [56] Subplot c) shows the workflow of post-processing the obtained WTmetaD trajectories by passing them through the full GNN model with the local decoder. The state labels are generated from the output prediction and consequently applied for computing the time series of free energy difference of solid states of interest (S) with respect to the molten phase M in subplot d). Computed standard errors are represented as shaded regions.

ns. The thermodynamically most stable configuration of iron is its BCC form with a free energy difference $-25 \pm 4 \text{ kJ/mol}$ relative to molten iron. The least stable FCC iron has a free energy difference of $65 \pm 3 \text{ kJ/mol}$ relative to molten iron. However, owing to strong finite size effects, it is more meaningful to draw qualitative comparisons to the experimental and computational works of literature. As reported in Ref.60, the experimental measured free energy difference between BCC and FCC iron, $\Delta G_{BCC-FCC}$, is 6.66 kJ/mol and $\Delta G_{FCC-HCP}$ is -2.22 kJ/mol at room temperature. Zero temperature calculations [61, 62] also show similar measures which are in good agreement with the stability rankings obtained in this work, $BCC > HCP > FCC$ iron in decreasing order.

III.B Nucleation of Glycine from Melt

The developed model is then assessed to a more complicated molecular system, glycine. Geometric data for zwitterionic glycine is slightly more intricate than that of iron (see Methods for detailed information). As more degrees of freedom are incorporated into the graphs of glycine molecules, a smaller neighborhood of individual molecules is defined with only 6 closest neighbors

($k = 6$). Intermolecular angles of characteristic vectors, ν_1, ν_2, ν_3 , and ν_4 are again expanded under basis functions which leads to 40-dimensional edge features between linked nodes.

Fig. 4 summarizes results from WTmetaD simulations biasing latent representations z_1, z_2 learnt by the GNN model. Several transitions can be identified by evaluating the time series in subplot a) along with multiple distinct wells in the reweighted free energy surface of (z_1, z_2) space (Fig. 4b)). However, after closely examining the obtained trajectories with visualization tools, we found that more polymorphic glycines were sampled even though the model was trained only on solid glycine in its three well-studied ambient products synthesized experimentally. These new polymorphs that our simulations visit have been however reported previously in Ref.45 and 66 as high-pressure structures. We thereby trained a new GNN model as a classifier on liquid glycine and all associated crystals including structures found under the effect of different pressures, and this leads to in total of six polymorphs namely α -, β -, γ -, δ -, ϵ -, and ζ -glycine. The notations for the solid glycines are adopted from Ref.66. Here, we only briefly describe the three additional glycine polymorphs since they are not the main focus of this work and their relative stabilities remain unclear: α -glycine

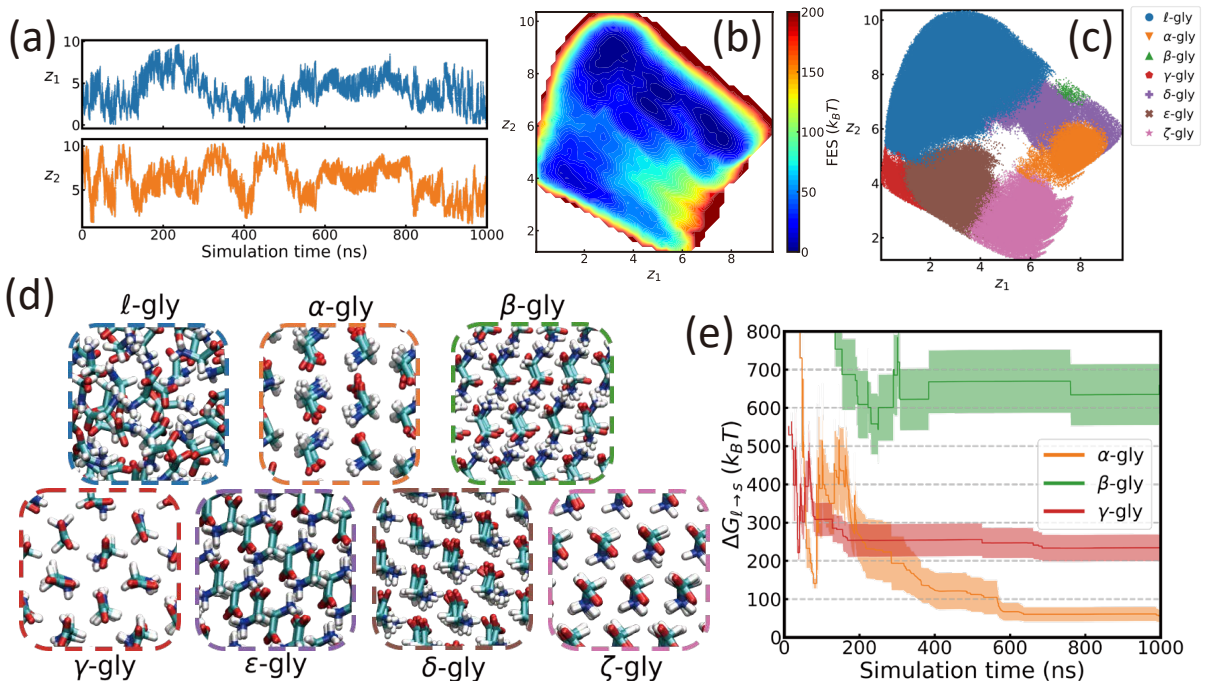


Figure 4. Results of WTmetaD simulations of the nucleation of glycine zwitterions. a) shows machine learnt latent representations z_1, z_2 vs. simulation time. Subplot b) shows reweighted FES (free energy surface) in the latent variable space (z_1, z_2) with multiple basins observed. Subplot c) is the scatter plot of liquid and solid glycines in (z_1, z_2) space classified by post-trained GNN model, and d) consists of snapshots to each corresponding class rendered from Visual Molecular Dynamics (VMD). [63] Free energy difference between states of interest vs. simulation time in e) shows convergence of the production runs. Standard errors are represented as shaded regions.

remains stable to pressures up to 23 GPa , meanwhile, β -glycine undergoes phase transition to δ -glycine ($P2_1/c$) at 0.8 GPa , γ -glycine transforms to ϵ -glycine (Pn) under application of pressure and the process complete at between 4 to 5 GPa , and decompression of ϵ -glycine leads to ζ -glycine ($I1$). [66, 67]

The distributions of individual glycine polymorphs are shown as scatter points in (z_1, z_2) space in Fig. 4c) with cutoff value $N_c = 65$, and the corresponding snapshots are provided in Fig. 4d). All observations above suggest the trained GNN latent representations capture the configurational information among various polymorphic structures of glycine molecules. Structures which are close to each other in configuration space (i.e. the associated high-pressure components) are sampled at ease with robust WTmetaD simulations.

The free energy difference $\Delta G_{\ell \rightarrow s}$ as a function of simulation time shown in Fig. 4e) is computed from Eq. 4 with a value of cutoff 65 which is set slightly larger than half of the population of glycine in the simulation cell. The figure is averaged over 9 independent runs of 1000 ns (see the SI for full $\Delta G_{\ell \rightarrow s}$ vs. simulation time plot) and the exact values are reported in Tab. III. This indicates the thermodynamic stability of ambient glycine polymorphs ranks in $\alpha\text{-gly} > \gamma\text{-gly} > \beta\text{-gly}$ at 500 K which is in consistent with the stability ranking reported in the literature which γ -gly is the most

thermodynamically stable at ambient temperature and the densest α -gly becomes the most stable at temperatures above 440 K . [67] In addition, we also identified a transition pathway of γ -gly to ϵ -gly to ζ -gly, while no direct transitions from γ -gly to ζ -gly, supported by 2-dimensional free energy analyses (see SI for details), which was also observed and reported experimentally. [68] Overall, this shows that the trained model is robust in learning structural properties for classifying configurations with simple graph convolution operations and readily computable features. Benefiting from the WTmetaD method, introducing biases along these low-dimensional latent representations validates the feasibility of obtaining relative free energy differences between competing allotropes/polymorphs starting only from their chemical identity and possible target structures.

IV CONCLUSION

Computational methods for investigating crystal nucleation have recently shown their strength in providing high temporal- and spatial-resolution descriptions. [69, 70] Due to the timescale limitations resulting from the rare event nature of nucleation, it is however necessary to perform enhanced sampling molecular dynamics. Most enhanced sampling methods involve biasing or fol-

lowing selected low-dimensional descriptors, and methods of constructing these descriptors remains to be an active field of research. Recent advancements in machine learning, particularly graph neural networks, have made it possible to achieve a better understanding of crystal nucleation from a perspective of learning relative slow modes [71], or on efficient computation of order parameters [24].

In this work, we have introduced a data-driven GNN-based representation learning model within an autoencoder framework to extract low-dimensional variables from configurational features found in experimental crystal structures. These variables serve as the key inputs for performing enhanced sampling methods. Our method employs straightforward convolutions and pooling techniques. To validate the usefulness of our machine learning pipeline, we studied nucleation of different allotropes and polymorphs of iron and glycine respectively from the melt. We biased the GNN based latent variables in well-tempered metadynamics and were able to achieve multiple back-and-forth state-to-state transitions and converged free energy estimates, both hallmarks of reliable sampling. This proves the robustness and potential of our graph neural network learnt variables for enhanced sampling. The thermodynamic stability rankings among allotropes or polymorphs are in agreement with experimental measures.

The protocol proposed here can be further improved in many ways, and here we highlight some possible avenues for future research. The current network only consists of convolution and pooling operations and it should be possible to introduce advanced manipulations on graph

data, such as the attention mechanism, to better interpolate and even extrapolate configurational information of complex species. [29, 33] Secondly, an obstacle to drawing quantitative comparisons to literature is due to finite size effects. To address this issue, various methods have been developed, including the introduction of constant chemical potential ensemble [72] and analytical correction under the classical nucleation framework [73–75]. In future work, we hope to combine data-driven approaches with those from statistical mechanics [76] to not just automate biasing variable discovery, as was done in this work, but also address finite size effects.

ACKNOWLEDGMENTS

Z.Z. thanks Prof. Mark E. Tuckerman, Prof. Omar Valsson, and Dr. Pablo M. Piaggi for useful advice. Z.Z. also thanks Dr. Zachary Smith and Dedi Wang for help in graph neural nets and C++. Z.Z. and P.T. thank Dr. Eric Beyerle, Dr. Bodhi P Vani, Dr. Yihang Wang, Dr. Sun-Ting Tsai, Dr. Luke Evans and Akashnathan Aranganathan for fruitful discussions and Dr. Eric Beyerle, Dedi Wang for proofreading the manuscript. This research was entirely supported by the U.S. Department of Energy, Office of Science, Basic Energy Sciences, CPIMS Program, under Award DE-SC0021009. We are also grateful to NSF ACCESS Bridges2 (project CHE180053) and University of Maryland Zaratán High-Performance Computing cluster for enabling the work performed in this work.

-
- [1] Hénin, J.; Lelièvre, T.; Shirts, M. R.; Valsson, O.; Delemotte, L. Enhanced sampling methods for molecular dynamics simulations. *arXiv preprint arXiv:2202.04164* **2022**,
 - [2] Laio, A.; Parrinello, M. Escaping free-energy minima. *Proceedings of the National Academy of Sciences* **2002**, *99*, 12562–12566.
 - [3] Torrie, G.; Valleau, J. Nonphysical sampling distributions in Monte Carlo free-energy estimation: Umbrella sampling. *Journal of Computational Physics* **1977**, *23*, 187–199.
 - [4] Allen, R. J.; Warren, P. B.; ten Wolde, P. R. Sampling Rare Switching Events in Biochemical Networks. *Phys. Rev. Lett.* **2005**, *94*, 018104.
 - [5] Bussi, G.; Laio, A. Using metadynamics to explore complex free-energy landscapes. *Nat. Rev. Phys.* **2020**, 1–13.
 - [6] Steinhardt, P. J.; Nelson, D. R.; Ronchetti, M. Bond-orientational order in liquids and glasses. *Phys. Rev. B* **1983**, *28*, 784.
 - [7] Santiso, E. E.; Trout, B. L. A general set of order parameters for molecular crystals. *The Journal of Chemical Physics* **2011**, *134*, 064109.
 - [8] Gavezzotti, A. Can a computer crystallize a liquid? Molecular simulation of continuous trajectories from liquid to crystalline n-hexane. *CrystEngComm* **2011**, *13*, 3573–3579.
 - [9] Salvalaglio, M.; Vetter, T.; Giberti, F.; Mazzotti, M.; Parrinello, M. Uncovering Molecular Details of Urea Crystal Growth in the Presence of Additives. *Journal of the American Chemical Society* **2012**, *134*, 17221–17233.
 - [10] Yi, P.; Locker, C. R.; Rutledge, G. C. Molecular dynamics simulation of homogeneous crystal nucleation in polyethylene. *Macromolecules* **2013**, *46*, 4723–4733.
 - [11] Giberti, F.; Tribello, G. A.; Parrinello, M. Transient polymorphism in NaCl. *Journal of chemical theory and computation* **2013**, *9*, 2526–2530.
 - [12] Piaggi, P. M.; Parrinello, M. Calculation of phase diagrams in the multithermal-multibaric ensemble. *The Journal of Chemical Physics* **2019**, *150*, 244119.
 - [13] Piaggi, P. M.; Valsson, O.; Parrinello, M. Enhancing Entropy and Enthalpy Fluctuations to Drive Crystallization in Atomistic Simulations. *Phys. Rev. Lett.* **2017**, *119*, 015701.
 - [14] Piaggi, P. M.; Parrinello, M. Predicting polymorphism in molecular crystals using orientational entropy. *Proceedings of the National Academy of Sciences* **2018**, *115*, 10251–10256.

- [15] Tsai, S.-T.; Smith, Z.; Tiwary, P. Reaction coordinates and rate constants for liquid droplet nucleation: Quantifying the interplay between driving force and memory. *The Journal of chemical physics* **2019**, *151*, 154106.
- [16] Finney, A. R.; Salvalaglio, M. Multiple pathways in NaCl homogeneous crystal nucleation. *Faraday Discussions* **2022**,
- [17] Giberti, F.; Salvalaglio, M.; Parrinello, M. Metadynamics studies of crystal nucleation. *IUCrJ* **2015**, *2*, 256–266.
- [18] Noé, F.; Tkatchenko, A.; Müller, K.-R.; Clementi, C. Machine learning for molecular simulation. *Annual review of physical chemistry* **2020**, *71*, 361–390.
- [19] Chen, M. Collective variable-based enhanced sampling and machine learning. *The European Physical Journal B* **2021**, *94*, 1–17.
- [20] Sarupria, S.; Hall, S. W.; Rogal, J. Machine learning for molecular simulations of crystal nucleation and growth. *MRS bulletin* **2022**, *47*, 949–957.
- [21] Beyerle, E. R.; Zou, Z.; Tiwary, P. Recent advances in describing and driving crystal nucleation using machine learning and artificial intelligence. *Current Opinion in Solid State and Materials Science* **2023**, *27*, 101093.
- [22] Mehdi, S.; Smith, Z.; Herron, L.; Zou, Z.; Tiwary, P. Enhanced Sampling with Machine Learning: A Review. *arXiv preprint arXiv:2306.09111* **2023**,
- [23] Jung, H.; Covino, R.; Arjun, A.; Leitold, C.; Delgado, C.; Bolhuis, P. G.; Hummer, G. Machine-guided path sampling to discover mechanisms of molecular self-organization. *Nature Computational Science* **2023**, 1–12.
- [24] Dietrich, F.; Rosas Advincola, X.; Gobbo, G.; Bellucci, M.; Salvalaglio, M. Machine Learning Nucleation Collective Variables with Graph Neural Networks. *ChemRxiv* **2023**,
- [25] Herrerger, N. S.; Dasetty, S.; Gandhi, D.; Lee, J.; Ferguson, A. L. Permutationally Invariant Networks for Enhanced Sampling (PINES): Discovery of Multi-Molecular and Solvent-Inclusive Collective Variables. *arXiv preprint arXiv:2308.08680* **2023**,
- [26] Elishav, O.; Podgaetsky, R.; Meikler, O.; Hirshberg, B. Collective Variables for Conformational Polymorphism in Molecular Crystals. *The Journal of Physical Chemistry Letters* **2023**, *14*, 971–976.
- [27] Gilmer, J.; Schoenholz, S. S.; Riley, P. F.; Vinyals, O.; Dahl, G. E. Neural message passing for quantum chemistry. International conference on machine learning. 2017; pp 1263–1272.
- [28] Schütt, K.; Kindermans, P.-J.; Sauceda Felix, H. E.; Chmiela, S.; Tkatchenko, A.; Müller, K.-R. Schnet: A continuous-filter convolutional neural network for modeling quantum interactions. *Advances in neural information processing systems* **2017**, *30*.
- [29] Xie, T.; Grossman, J. C. Crystal graph convolutional neural networks for an accurate and interpretable prediction of material properties. *Physical review letters* **2018**, *120*, 145301.
- [30] Jørgensen, P. B.; Jacobsen, K. W.; Schmidt, M. N. Neural message passing with edge updates for predicting properties of molecules and materials. *arXiv preprint arXiv:1806.03146* **2018**,
- [31] DeFever, R. S.; Targonski, C.; Hall, S. W.; Smith, M. C.; Sarupria, S. A generalized deep learning approach for local structure identification in molecular simulations. *Chemical science* **2019**, *10*, 7503–7515.
- [32] Moradzadeh, A.; Oliaei, H.; Aluru, N. R. Topology-Based Phase Identification of Bulk, Interface, and Confined Water Using an Edge-Conditioned Convolutional Graph Neural Network. *The Journal of Physical Chemistry C* **2023**, *127*, 2612–2621.
- [33] Banik, S.; Dhabal, D.; Chan, H.; Manna, S.; Cherukara, M.; Molinero, V.; Sankaranarayanan, S. K. CEGANN: Crystal Edge Graph Attention Neural Network for multiscale classification of materials environment. *npj Computational Materials* **2023**, *9*, 23.
- [34] Kim, Q.; Ko, J.-H.; Kim, S.; Jhe, W. GCIceNet: a graph convolutional network for accurate classification of water phases. *Physical Chemistry Chemical Physics* **2020**, *22*, 26340–26350.
- [35] Fulford, M.; Salvalaglio, M.; Molteni, C. DeepIce: A deep neural network approach to identify ice and water molecules. *Journal of Chemical Information and Modeling* **2019**, *59*, 2141–2149.
- [36] Pietrucci, F.; Andreoni, W. Graph theory meets ab initio molecular dynamics: atomic structures and transformations at the nanoscale. *Physical review letters* **2011**, *107*, 085504.
- [37] Bartók, A. P.; Kondor, R.; Csányi, G. On representing chemical environments. *Physical Review B* **2013**, *87*, 184115.
- [38] Tribello, G. A.; Giberti, F.; Sosso, G. C.; Salvalaglio, M.; Parrinello, M. Analyzing and Driving Cluster Formation in Atomistic Simulations. *Journal of Chemical Theory and Computation* **2017**, *13*, 1317–1327.
- [39] Sipka, M.; Erlebach, A.; Grajciar, L. Constructing Collective Variables Using Invariant Learned Representations. *Journal of Chemical Theory and Computation* **2023**, *19*, 887–901.
- [40] Fix, E.; Hodges, J. L. Discriminatory analysis. Nonparametric discrimination: Consistency properties. *International Statistical Review/Revue Internationale de Statistique* **1989**, *57*, 238–247.
- [41] Simonovsky, M.; Komodakis, N. Dynamic edge-conditioned filters in convolutional neural networks on graphs. Proceedings of the IEEE conference on computer vision and pattern recognition. 2017; pp 3693–3702.
- [42] Jia, X.; De Brabandere, B.; Tuytelaars, T.; Gool, L. V. Dynamic filter networks. *Advances in neural information processing systems* **2016**, *29*.
- [43] Eppstein, D.; Paterson, M. S.; Yao, F. F. On nearest-neighbor graphs. *Discrete & Computational Geometry* **1997**, *17*, 263–282.
- [44] Gražulis, S.; Chateigner, D.; Downs, R. T.; Yokochi, A. F. T.; Quirós, M.; Lutterotti, L.; Manakova, E.; Butkus, J.; Moeck, P.; Le Bail, A. Crystallography Open Database – an open-access collection of crystal structures. *Journal of Applied Crystallography* **2009**, *42*, 726–729.
- [45] Dawson, A.; Allan, D. R.; Belmonte, S. A.; Clark, S. J.; David, W. I.; McGregor, P. A.; Parsons, S.; Pulham, C. R.; Sawyer, L. Effect of high pressure on the crystal structures of polymorphs of glycine. *Crystal growth & design* **2005**, *5*, 1415–1427.
- [46] Iitaka, Y. The crystal structure of β -glycine. *Acta Crystallographica* **1960**, *13*, 35–45.
- [47] Macrae, C. F.; Sovago, I.; Cottrell, S. J.; Galek, P. T.; McCabe, P.; Pidcock, E.; Platings, M.; Shields, G. P.; Stevens, J. S.; Towler, M.; others Mercury 4.0: From visualization to analysis, design and prediction. *Journal*

- of applied crystallography **2020**, *53*, 226–235.
- [48] Valsson, O.; Tiwary, P.; Parrinello, M. Enhancing important fluctuations: Rare events and metadynamics from a conceptual viewpoint. *Annual review of physical chemistry* **2016**, *67*, 159–184.
- [49] Thompson, A. P.; Aktulga, H. M.; Berger, R.; Bolintineanu, D. S.; Brown, W. M.; Crozier, P. S.; in 't Veld, P. J.; Kohlmeyer, A.; Moore, S. G.; Nguyen, T. D.; Shan, R.; Stevens, M. J.; Tranchida, J.; Trott, C.; Plimpton, S. J. LAMMPS - a flexible simulation tool for particle-based materials modeling at the atomic, meso, and continuum scales. *Comp. Phys. Comm.* **2022**, *271*, 108171.
- [50] Berendsen, H. J.; van der Spoel, D.; van Drunen, R. GROMACS: a message-passing parallel molecular dynamics implementation. *Comp. Phys. Commun.* **1995**, *91*, 43–56.
- [51] Bonomi, M.; Bussi, G.; Camilloni, C. C. Promoting transparency and reproducibility in enhanced molecular simulations. *Nat. Methods.* **2019**, *16*, 670–673.
- [52] Tribello, G. A.; Bonomi, M.; Branduardi, D.; Camilloni, C.; Bussi, G. PLUMED 2: New feathers for an old bird. *Comp. Phys. Comm.* **2014**, *185*, 604–613.
- [53] Lynch, J. W. Molecular Structure and Function of the Glycine Receptor Chloride Channel. *Physiological Reviews* **2004**, *84*, 1051–1095, PMID: 15383648.
- [54] Boldyreva, E.; Drebuschak, V.; Drebuschak, T.; Paukov, I.; Kovalevskaya, Y. A.; Shutova, E. Polymorphism of glycine, Part I. *Journal of thermal analysis and calorimetry* **2003**, *73*, 409–418.
- [55] Stukowski, A. Visualization and analysis of atomistic simulation data with OVITO-the Open Visualization Tool. *MODELLING AND SIMULATION IN MATERIALS SCIENCE AND ENGINEERING* **2010**, *18*.
- [56] Stukowski, A. Structure identification methods for atomistic simulations of crystalline materials. *Modelling and Simulation in Materials Science and Engineering* **2012**, *20*, 045021.
- [57] Lee, T.; Baskes, M. I.; Valone, S. M.; Doll, J. Atomistic modeling of thermodynamic equilibrium and polymorphism of iron. *Journal of Physics: Condensed Matter* **2012**, *24*, 225404.
- [58] Ou, X. Molecular dynamics simulations of fcc-to-bcc transformation in pure iron: A review. *Materials Science and Technology* **2017**, *33*, 822–835.
- [59] Tiwary, P.; Parrinello, M. A time-independent free energy estimator for metadynamics. *The Journal of Physical Chemistry B* **2015**, *119*, 736–742.
- [60] Guillermet, A. F.; Gustafson, P. An Assessment of the Thermodynamic Properties and the(p, T) Phase Diagram of Iron. *High Temp.–High Press.* **1984**, *16*, 591–610.
- [61] Etesami, S. A.; Asadi, E. Molecular dynamics for near melting temperatures simulations of metals using modified embedded-atom method. *Journal of Physics and Chemistry of Solids* **2018**, *112*, 61–72.
- [62] Lee, B.-J.; Baskes, M. I. Second nearest-neighbor modified embedded-atom-method potential. *Physical Review B* **2000**, *62*, 8564.
- [63] Humphrey, W.; Dalke, A.; Schulten, K. VMD: Visual molecular dynamics. *Journal of Molecular Graphics* **1996**, *14*, 33–38.
- [64] Honeycutt, J. D.; Andersen, H. C. Molecular dynamics study of melting and freezing of small Lennard-Jones clusters. *Journal of Physical Chemistry* **1987**, *91*, 4950–4963.
- [65] Faken, D.; Jónsson, H. Systematic analysis of local atomic structure combined with 3D computer graphics. *Computational Materials Science* **1994**, *2*, 279–286.
- [66] Bull, C. L.; Flowitt-Hill, G.; de Gironcoli, S.; Küçükbenli, E.; Parsons, S.; Pham, C. H.; Playford, H. Y.; Tucker, M. G. ζ -Glycine: insight into the mechanism of a polymorphic phase transition. *IUCrJ* **2017**, *4*, 569–574.
- [67] Boldyreva, E. Glycine: The gift that keeps on giving. *Israel Journal of Chemistry* **2021**, *61*, 828–850.
- [68] Goryainov, S.; Boldyreva, E.; Kolesnik, E. Raman observation of a new (ζ) polymorph of glycine? *Chemical Physics Letters* **2006**, *419*, 496–500.
- [69] Sosso, G. C.; Chen, J.; Cox, S. J.; Fitzner, M.; Pedevilla, P.; Zen, A.; Michaelides, A. Crystal nucleation in liquids: Open questions and future challenges in molecular dynamics simulations. *Chemical reviews* **2016**, *116*, 7078–7116.
- [70] Blow, K. E.; Quigley, D.; Sosso, G. C. The seven deadly sins: When computing crystal nucleation rates, the devil is in the details. *The Journal of Chemical Physics* **2021**, *155*.
- [71] Liu, B.; Xue, M.; Qiu, Y.; Konovalov, K. A.; O'Connor, M. S.; Huang, X. GraphVAMPnets for uncovering slow collective variables of self-assembly dynamics. *The Journal of Chemical Physics* **2023**, *159*.
- [72] Karmakar, T.; Finney, A. R.; Salvalaglio, M.; Yazaydin, A. O.; Perego, C. Non-Equilibrium Modeling of Concentration-Driven processes with Constant Chemical Potential Molecular Dynamics Simulations. *Accounts of Chemical Research* **2023**, *56*, 1156–1167.
- [73] Salvalaglio, M.; Perego, C.; Giberti, F.; Mazzotti, M.; Parrinello, M. Molecular-dynamics simulations of urea nucleation from aqueous solution. *Proceedings of the National Academy of Sciences* **2015**, *112*, E6–E14.
- [74] Salvalaglio, M.; Tiwary, P.; Maggioni, G. M.; Mazzotti, M.; Parrinello, M. Overcoming time scale and finite size limitations to compute nucleation rates from small scale well tempered metadynamics simulations. *The Journal of Chemical Physics* **2016**, *145*, 211925.
- [75] Hussain, S.; Haji-Akbari, A. How to quantify and avoid finite size effects in computational studies of crystal nucleation: The case of homogeneous crystal nucleation. *The Journal of Chemical Physics* **2022**, *156*, 054503.
- [76] Wang, Y.; Herron, L.; Tiwary, P. From data to noise to data for mixing physics across temperatures with generative artificial intelligence. *Proceedings of the National Academy of Sciences* **2022**, *119*, e2203656119.